Production of axial-vector mesons at e^+e^- collisions with double-tagging as a way to constrain the axial meson light-by-light contribution to the muon g-2 and the hyperfine splitting of muonic hydrogen

Antoni Szczurek*

Institute of Nuclear Physics, Polish Academy of Sciences, ul. Radzikowskiego 152, PL-31-342 Kraków, Poland

(Received 23 June 2020; accepted 21 November 2020; published 28 December 2020)

We calculate cross sections for production of axial-vector $f_1(1285)$ mesons for double-tagged measurements of the $e^+e^- \to e^+e^- f_1(1285)$ reaction. Different $\gamma^*\gamma^* \to f_1(1285)$ vertices from the literature are used. Both integrated cross section as well as differential distributions are calculated. Predictions for a potential measurement at Belle II are presented. Quite different results are obtained for the different vertices proposed in the literature. Several observables are discussed. The distribution in photon virtuality asymmetry is especially sensitive to the $\gamma^*\gamma^* \to f_1$ vertex. Future measurements at e^+e^- colliders could test and/or constrain the $\gamma^*\gamma^* \to f_1(a_1, f_1')$ vertices and associated form factors, known to be important ingredients for calculating contributions to anomalous magnetic moment of muon and hyperfine splitting of levels of muonic atoms. In addition we present helicity amplitudes as a function of both photon virtualities. Only some amplitudes are different from zero. Different models have different relative size of LT, TL, and TT amplitudes.

DOI: 10.1103/PhysRevD.102.113015

I. INTRODUCTION

The coupling of neutral mesons to two photons is an important ingredient of mesonic physics. In Ref. [1] tensorial coupling was discussed for different types of mesons (pseudoscalar, scalar, axial-vector, and tensor). In general, the amplitudes can be expressed in terms of functions of photon virtualities often called transition form factors. They were tested in details for pseudoscalar mesons (π^0, η, η'). Recently there was discussion how to calculate such objects for pseudoscalar [2] and scalar [3] quarkonia.

The axial vector mesons and in particular their coupling to photons [4] are very important in the context of their contribution to anomalous magnetic moment of muon [5–10].

The anomalous magnetic moment of muon is one of the most fundamental quantities in particle physics (see, e.g., [11,12]). A first calculation of QED corrections to anomalous magnetic moment was performed long ago [13]. Recent state of the art can be found, e.g., in [11,12,14]. The current precision of QED calculation is so high that hadronic contributions to muon anomalous moment must be included. The so-called light-by-light (LbL) contributions are very important but rather uncertain. The coupling $\gamma^*\gamma^* \to f_1(1285)$ is one of the most uncertain ingredients. Different couplings have been suggested in the literature.

Recently the contribution of the $\gamma^*\gamma^* \to f_1(1285)$ coupling was identified and included in calculating hyperfine splitting of levels of muonic hydrogen, and turned out to be quite sizeable [15]. These are rather fundamental problems and better constraints on $\gamma^*\gamma^*$ coupling are badly needed.

In calculating $\delta a_\mu^{f_1}$ one often writes:

$$\delta a_\mu^{f_1} = \int dQ_1^2 dQ_2^2 \rho_\mu^{f_1}(Q_1^2, Q_2^2), \tag{1.1}$$

where $\rho_\mu^{f_1}(Q_1^2, Q_2^2)$ is the density of the f_1 contribution to the muon anomalous magnetic moment. The integrand of (1.1) (called often density for brevity) peaks at $Q_1^2, Q_2^2 \sim 0.5$ GeV^2 and gives almost negligible contribution for $Q_1^2, Q_2^2 > 1.5$ GeV^2, see, e.g., [7].

The $\gamma^*\gamma^* f_1(1285)$ coupling can be also quite important for hyperfine splitting of levels of muonic hydrogen [15]. It is also very important to calculate rare decays such as $f_1(1285) \to e^+e^-$ [16,17]. There both spacelike and timelike photons enter corresponding loop integral(s) so one tests both regions simultaneously. The corresponding branching fraction is very small ($BF \sim 10^{-8}$). The same loop integral enters the production of f_1 in

*Also at University of Rzeszów, PL-35-959 Rzeszów, Poland. antoni.szczurek@ifj.edu.pl

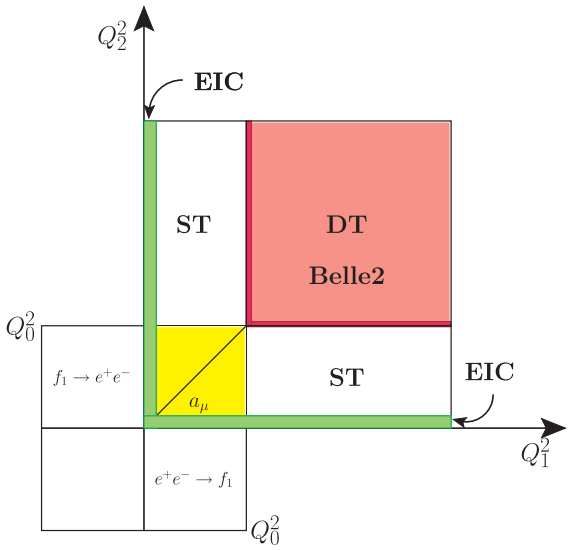

FIG. 1. Possible tests of the $\gamma^*\gamma^* \to AV$ vertex in the (Q_1^2, Q_2^2) space: contribution to $g-2$, hyperfine splitting of muonic hydrogen, EIC, $f_1 \to e^+e^-$ or $e^+e^- \to f_1$ and DT in e^+e^- collisions discussed in the present paper in extent.

electron-positron annihilation [16,17]. There is already a first evidence of such a process from the SND collaboration at VEPP-2000 [18]. The $f_1(1285)$ was also observed in $\gamma p \to f_1(1285)p$ reaction by the CLAS collaboration [19]. The experimental results do not agree with theoretical predictions [20–22].

Figure 1 illustrates how different regions of the vertex functions are tested in different processes. The square $(0, Q_0^2)x(0, Q_0^2)$ close to the origin shows the region where the dominant contributions to $g-2$ comes from. The square $(Q_0^2, \infty)x(Q_0^2, \infty)$ marked in red represents the region which can be tested in double-tagging experiments. The short diagonal $(Q_1^2 = Q_2^2)$ line represents region important for hyperfine splitting of levels of muonic hydrogen. The narrow strips along the x and y axis shows a possibility to study production of $f_1(1285)$ in $e+A$ collisions at EIC. Marked is also the region of photon virtualities which contributes to $f_1 \to e^+e^-$ or to the production of $f_1(1285)$ in e^+e^- annihilation.

In the present paper we suggest how to limit the behavior of the $\gamma^*\gamma^* \to f_1(1285)$ coupling(s)[1] at somewhat larger photon virtualities accessible at double-tagged $e^+e^- \to e^+e^-f_1(1285)$ measurements, where typically $Q_1^2, Q_2^2 > Q_0^2 = 2$ GeV^2.

II. SOME DETAILS OF THE MODEL CALCULATIONS

Figure 2 shows the Feynman diagram for axial-vector meson production in e^+e^- collisions. The small circle in the middle represents the $\gamma^*\gamma^* \to AV$ vertex tested in double-tagging experiment.

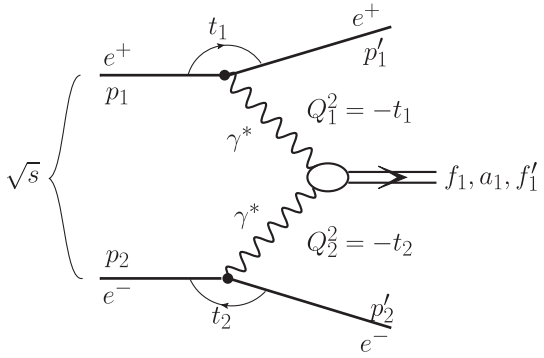

FIG. 2. The generic diagram for $e^+e^- \to e^+e^-AV$ and kinematical variables used in this paper.

A. $\gamma^*\gamma^* \to f_1(1285)$ vertices

In the formalism presented, e.g., in [4] the covariant matrix element for $\gamma^*\gamma^* \to f_1(1285)$ is written as:

$$R^{\mu,\nu} = -g^{\mu\nu} + \frac{1}{X}[(q_1\dot{q}_2)(q_1^\mu q_2^\nu + q_2^\mu q_1^\nu) - q_1^2 q_2^\mu q_2^\nu - q_2^2 q_1^\mu q_1^\nu], \tag{2.1}$$

where

$$X = (q_1\dot{q}_2) - q_1^2 q_2^2 = \frac{M_f^4}{4}\left(1 + \frac{2(q_{1t}^2 + q_{2t}^2)}{M_f^2} + \frac{(q_{1t}^2 - q_{2t}^2)^2}{M_f^4}\right). \tag{2.2}$$

1. DKMMR2019 vertex

In Ref. [15] the vertex was written as:

$$\begin{aligned} T_\alpha^{\mu\nu} = 4\pi\alpha_{em}\epsilon_{\rho\sigma\tau\alpha}\Big\{ & R^{\mu\rho}(q_1,q_2)R^{\nu\sigma}(q_1,q_2) \\ & \times (q_1-q_2)^\tau \nu F^0(q_1^2,q_2^2) \\ & + R^{\nu\rho}(q_1,q_2)\left(q_1^\mu - \frac{q_1^2}{\nu}q_2^\mu\right) q_1^\sigma q_2^\tau F^{(1)}(q_1^2,q_2^2) \\ & + R^{\mu\rho}(q_1,q_2)\left(q_2^\nu - \frac{q_2^2}{\nu}q_1^\nu\right) q_2^\sigma q_1^\tau F^{(1)}(q_2^2,q_1^2)\Big\}, \end{aligned} \tag{2.3}$$

where

$$\nu = (q_1 q_2) = \frac{1}{2}((q_1+q_2)^2 - q_1^2 - q_2^2). \tag{2.4}$$

In the nonrelativistic model

$$F^{(0)}(0,0) = -F^{(1)}(0,0). \tag{2.5}$$

We use the normalization of form factors

[1]The same is true for other axial-vector (a_1, f_1') mesons.

$$F^{(0)}(0,0) = 0.266\ \text{GeV}^{-2}. \tag{2.6}$$

In [15] the vertex was supplemented by the following factorized dipole form factor

$$F_{DKMMR}(Q_1^2, Q_2^2) = \frac{\Lambda_D^4}{(\Lambda_D^2 + Q_1^2)^2}\frac{\Lambda_D^4}{(\Lambda_D^2 + Q_2^2)^2}. \tag{2.7}$$

The $\Lambda_D \approx 1$ GeV was suggested as being consistent with the L3 collaboration data [23].

We will ascribe also the name NQM (nonrelativistic quark model) to this vertex.

2. OPV2018 vertex

In Ref. [6] the vertex function for $\gamma^*\gamma^* \to f_1$ was constructed based on an analysis of the $f_1(1285) \to \rho^0\gamma$ decay within NJL model with triangle pointlike quark-antiquark meson coupling and using vector meson dominance picture when passing from $\rho^0\gamma$ to $\gamma^*\gamma^*$. The corresponding vertex for two-photon coupling there [see their formula (40)] was derived to be

$$\begin{aligned} T^{\mu\nu\alpha} = iC_{OPV}\{&\epsilon^{\mu\nu\sigma\alpha}(q_{1,\sigma}((q_1q_2) + 2q_1^2) \\ &- q_{2,\sigma}((q_1q_2) + 2q_2^2)) \\ &+ \epsilon^{\rho\sigma\nu\alpha}q_{2,\rho}q_{1,\sigma}(q_2 + 2q_1)^\mu \\ &+ \epsilon^{\rho\sigma\mu\alpha}q_{1,\rho}q_{2,\sigma}(q_1 + 2q_2)^\nu\} \end{aligned} \tag{2.8}$$

when limiting to third powers of momenta. Above

$$C_{OPV} = \frac{5\alpha_{em}g_\rho}{36\pi m_q^2}, \tag{2.9}$$

where m_q is effective (constituent) quark mass. In [6] it was set to $m_q = 0.28$ GeV. Of course the results strongly depend on the value. The value of g_ρ is explicitly given in [6].

In the OPV approach is based on calculation of the triangle loop. In this approach the form factor is believed to be included already in the amplitude given in [6] and the extra form factor is in principle not needed. We will return to the issue in the Result section, especially in the context of double-tagging in $e^+e^- \to e^+e^-f_1$ reaction.

3. LR2019 vertex

Finally we consider also the vertex used very recently in [9]. In this approach the vertex is

$$\begin{aligned} T^{\mu\nu\rho} \propto \epsilon^{\alpha\beta\rho\sigma}\{&(q_1^2\delta_\alpha^\mu - q_{1,\alpha}q_1^\mu)q_2^\sigma\delta_\beta^\nu A(Q_1^2, Q_2^2) \\ &- (q_2^2\delta_\beta^\nu - q_{2,\beta}q_2^\nu)q_1^\sigma\delta_\alpha^\mu A(Q_2^2, Q_1^2)\}. \end{aligned} \tag{2.10}$$

The normalization was also given there. It was pointed out that the $A(Q_1^2, Q_2^2)$ function does not need to be symmetric under exchange of Q_1^2 and Q_2^2. Actually asymmetric form factors calculated from the hard wall and Sakai-Sugimoto models were used there. In our evaluation here we will use hard wall (HW2) form factors as well as factorized dipole symmetric/asymmetric form factors as specified below to illustrate the effect of the holographic approach. The HW2 form factor can be sufficiently well represented as:

$$\begin{aligned} A(Q_1^2, Q_2^2) &\approx A(0,0)F_S(Q_1^2)F_L(Q_2^2), \\ A(Q_2^2, Q_1^2) &\approx A(0,0)F_L(Q_1^2)F_S(Q_2^2), \end{aligned} \tag{2.11}$$

where

$$\begin{aligned} F_S(Q^2) &= \left(\frac{\Lambda_S^2}{\Lambda_S^2 + Q^2}\right)^2, \\ F_L(Q^2) &= \left(\frac{\Lambda_L^2}{\Lambda_L^2 + Q^2}\right)^2, \end{aligned} \tag{2.12}$$

where $\Lambda_L > \Lambda_S$. We show the HW2 form factor and its factorized dipole approximate representation as a function of $(\log_{10}(Q_1^2), \log_{10}(Q_2^2))$ in Fig. 3.

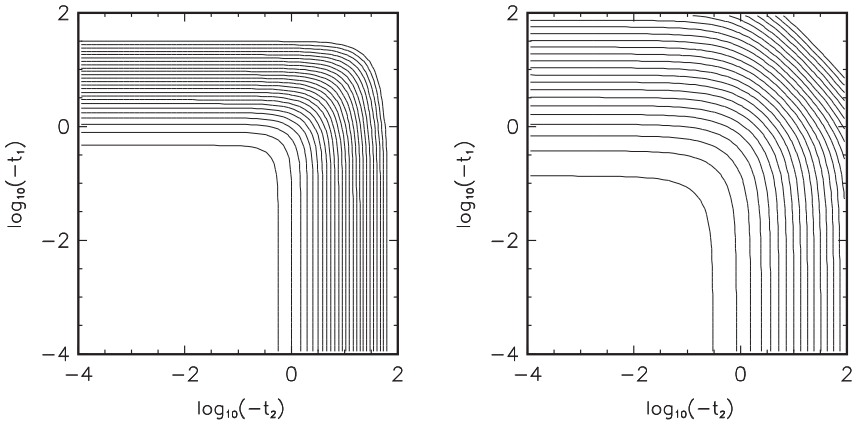

FIG. 3. Maps of the original (left panel) and parametrized (right panel) HW2 form factor $A(Q_1^2, Q_2^2)/A(0,0)$ as a function of $[\log_{10}(Q_1^2), \log_{10}(Q_2^2)]$. In the latter case $\Lambda_S = 0.8$ GeV and $\Lambda_L = 1.2$ GeV.

4. RS2019 vertex

In Ref. [8] a vertex based on RχT approach was considered. In this approach one gets:

$$T^{\mu\nu\alpha} = e^2 F_{RS}(q_1,q_2)\{i\epsilon^{\mu\tau\alpha\rho} q_{1,\rho}(q_2^\nu q_{2,\tau} - g_\tau^\nu q_2^2) - i\epsilon^{\nu\tau\alpha\rho} q_{2,\rho}(q_1^\mu q_{1,\tau} - g_\tau^\mu q_1^2) + i\epsilon^{\mu\nu\rho\sigma} q_{1,\rho} q_{2,\sigma}(q_1^\alpha - q_2^\alpha)\}. \quad (2.13)$$

Above we have denoted:

$$F_{RS}(q_1,q_2) = \frac{2c_A}{M_A}\frac{(q_1^2 - q_2^2)}{(q_1^2 - M_V^2)(q_2^2 - M_V^2)}. \quad (2.14)$$

The c_A is defined in [8]. $M_V \approx m_\rho \approx m_\omega = 0.8$ GeV. The reader is asked to note vanishing of F_{RS} at $Q_1^2 = Q_2^2$. This, as will be discussed below, has important consequences for the double tagged measurements.

The form factor used in RS2019 are antisymmetric. Additional symmetric form factors arising at higher order were discussed in a revised version of [8] (see Appendix C there). In the following we will use the lower order result to illustrate the situation.

It was ascertained recently in [24] that the RχT approach provides only purely transverse axial-vector meson contributions.

5. MR2019 vertex

In Ref. [17] the following vertex was used (we change a bit notation to be consistent with our previous formulae)

$$T^{\mu\nu\alpha} = \frac{i}{m_{f_1}^2}\epsilon^{\mu\nu\rho\sigma}\{F(q_1^2,q_2^2) q_{2\rho} q_{1,\sigma}(q_1 - q_2)^\alpha - q_2^2 G(q_1^2,q_2^2)\delta_\rho^\alpha q_{1,\sigma} + q_1^2 G(q_2^2,q_1^2)\delta_\rho^\alpha q_{2,\sigma}\} \quad (2.15)$$

to the production of $f_1(1285)$ in the e^+e^- annihilation. Since in this case both spacelike and timelike virtualities enter the calculation of the relevant matrix element the form factors had to be generalized. In [17] the form factors were parametrized in the spirit of vector meson dominance approach as:

$$G(q_1^2,q_2^2) = \frac{g_2 M_f^5}{q(q_1^2 - m_\rho^2 + im_\rho\Gamma_\rho)(q_2^2 - m_\rho^2 + im_\rho\Gamma_\rho)}, \quad (2.16)$$

$$F(q_1^2,q_2^2) = \frac{g_1 M_f^3 (q_2^2 - q_1^2)}{q(q_1^2 - m_\rho^2 + im_\rho\Gamma_\rho)(q_2^2 - m_\rho^2 + im_\rho\Gamma_\rho)}. \quad (2.17)$$

One can see the characteristic ρ meson propagators. The $F(q_1^2,q_2^2)$ form factor is asymmetric with respect to q_1^2 and q_2^2 exchange to assure Bose symmetry of the amplitude. An extra q in the denominator was attached to the VDM-like vertex to assure "correct" behavior of the form factors at large photon virtualities [1]. Of course, it is not obvious that such a correction should enter in the multiplicative manner. The coupling constant

$$g_2 = (2.9 \pm 0.4) \times 10^{-4} \quad (2.18)$$

was found in [17]. It was allowed in [17] for g_2 to be complex. It was argue that $|g_1| \sim g_2$ to describe the first $e^+e^- \to f_1(1285)$ data from VEPP-2000 [18]. We shall show in this paper how important is the interference of both terms in the DT case.

6. LLNRS vertex

Recently we have proposed a new parametrization of the $\rho^0\rho^0 \to f_1$ and $\omega\omega \to f_1$ vertices [25] important for the mechanism of f_1 production in pp or $p\bar{p}$ collisions at low and intermediate energies. The corresponding vertex for auxiliary angular momenta l,S = 2,2 reads:

$$i\Gamma_{\mu\nu\alpha}^{VV\to f_1} = \frac{2g_{VVf_1}}{M_0^4} F_{VV\to f_1}(q_1,q_2)[(q_1 - q_2)^\rho (q_1 - q_2)^\sigma \epsilon_{\lambda\sigma\alpha\beta} k^\beta (q_{1\kappa}\delta_\mu^\lambda - q_1^\lambda g_{\kappa\mu})(q_2^\kappa g_{\rho\nu} - q_{2\rho}\delta_\nu^\kappa) + (q_1 \leftrightarrow q_2, \mu \leftrightarrow \nu)]. \quad (2.19)$$

In this parametrization $M_0 = 1$ GeV is set arbitrarily for dimensional reasons.

The coupling constant $g_{\rho^0\rho^0 f_1}$ can be obtained, e.g., from the decay of $f_1 \to 2(\pi^+\pi^-)$ [26]. $g_{\rho\rho f_1} \approx 20$–$30$ is found from adjusting to the experimental branching fraction for $f_1 \to 2(\pi^+\pi^-)$. Much smaller value $g_{\rho\rho f_1} \approx 10$ is obtained from $f_1 \to \rho^0\gamma$ decays. The difference is most probably due to $f_1 \to a_1^\pm\pi^\mp \to 2(\pi^+\pi^-)$ decay mode. Assuming SU(2) flavor relation between ρ^0 and ω flavor wave functions one may expect $g_{\omega\omega f_1} = g_{\rho^0\rho^0 f_1}$.

The form factor in (2.19) is parametrized in [26] as:

$$F_{VV\to f_1}(t_1,t_2) = \frac{\Lambda_D^4}{\Lambda_D^4 + (t_1 - m_V^2)^2}\frac{\Lambda_D^4}{\Lambda_D^4 + (t_2 - m_V^2)^2}. \quad (2.20)$$

or alternatively

$$F_{VV\to f_1}(t_1,t_2)=\exp\left(\frac{t_1-m_V^2}{\Lambda_E^2}\right)\exp\left(\frac{t_2-m_V^2}{\Lambda_E^2}\right). \quad (2.21)$$

The form factor is normalized when $V=\rho$, ω meson is on mass shell. The form factor parameters Λ_D or Λ_E are in general not well known.

When supplementing the hadronic vertices by the VDM idea it can be used also for the $\gamma^*\gamma^*\to f_1$ production discussed here.

Then one can write:

$$i\Gamma_{\mu\nu\alpha}^{\gamma^*\gamma^*\to f_1}=\left(\frac{e}{\gamma_\rho}\right)^2 F_{\rho\rho\to f_1}(t_1,t_2)\,i\Gamma_{\mu\nu\alpha}^{\rho^0\rho^0\to f_1}\frac{m_\rho^2}{m_\rho^2+Q_1^2}\frac{m_\rho^2}{m_\rho^2+Q_2^2}+\left(\frac{e}{\gamma_\omega}\right)^2 F_{\omega\omega\to f_1}(t_1,t_2)\,i\Gamma_{\mu\nu\alpha}^{\omega\omega\to f_1}\frac{m_\omega^2}{m_\omega^2+Q_1^2}\frac{m_\omega^2}{m_\omega^2+Q_2^2}. \quad (2.22)$$

The $\gamma^*\gamma^*\to f_1$ can be then obtained by using γ_ρ and γ_ω constants from [27]. The reader may recognize the VDM-like factors $\frac{m_V^2}{m_V^2+Q_1^2}$ and $\frac{m_V^2}{m_V^2+Q_2^2}$ for each of the photon. We will return to the issue when discussing helicity-dependent matrix elements in the Result section.

B. General requirements

Any correct formulation of the $\gamma^*\gamma^*\to f_1(1285)$ vertex must fulfill at least three general requirements:

(i) Gauge invariance requires:

$$q_{1\mu}T^{\mu\nu\alpha}=q_{2\nu}T^{\mu\nu\alpha}=0, \quad (2.23)$$

(ii) Landau-Yang theorem [28] requires:

$$T^{\mu\nu\alpha}\to 0 \quad \text{when } q_1^2\to 0 \quad \text{and} \quad q_2^2\to 0. \quad (2.24)$$

(iii) Bose symmetry implies

$$T^{\mu\nu\alpha}(q_1,q_2)=T^{\nu\mu\alpha}(q_2,q_1) \quad (2.25)$$

which for our reaction means, e.g.:

$$\frac{d\sigma(t_1,t_2;y,\phi)}{dt_1dt_2dyd\phi}=\frac{d\sigma(t_2,t_1;y,\phi)}{dt_1dt_2dyd\phi} \quad (2.26)$$

for each y,ϕ.

Some vertices fulfill also

$$T^{\mu\nu\alpha}p_\alpha=0, \quad (2.27)$$

where p is four-momentum of the axial-vector meson. This automatically guarantees that only spin-1 particle f_1 is involved and unphysical states are ignored. A related discussion can be found, e.g., in [27].

C. Form factors

Some of the $F(Q_1^2,Q_2^2)$ form factors can be constraint from the so-called decay width into transverse and longitudinal photon, some are poorly know as they cannot be obtained as they do not enter the formula for the radiative decay width. The radiative decay width is known [29] and is

$$\tilde{\Gamma}_{\gamma\gamma}=3.5\ \text{keV}. \quad (2.28)$$

Then some of the form factors are parametrized as:

$$F(Q_1^2,Q_2^2)=\left(\frac{\Lambda_M^2}{\Lambda_M^2+Q_1^2}\right)\left(\frac{\Lambda_M^2}{\Lambda_M^2+Q_2^2}\right), \quad (2.29)$$

$$F(Q_1^2,Q_2^2)=\left(\frac{\Lambda_D^2}{\Lambda_D^2+Q_1^2}\right)^2\left(\frac{\Lambda_D^2}{\Lambda_D^2+Q_2^2}\right)^2, \quad (2.30)$$

$$F(Q_1^2,Q_2^2)=\left(\frac{\Lambda_M^2}{Q_1^2+Q_2^2+\Lambda_M^2}\right), \quad (2.31)$$

$$F(Q_1^2,Q_2^2)=\left(\frac{\Lambda_D^2}{Q_1^2+Q_2^2+\Lambda_D^2}\right)^2. \quad (2.32)$$

Both monopole and dipole parametrizations of form factors will be used in the following. We will call the first two as factorized Ansatze and the next two as pQCD inspired powerlike parametrizations.

In general, the form factors in Eqs. (2.10) do not need to be symmetric with respect to Q_1^2 and Q_2^2 exchange [9]. For example in Ref. [9] asymmetric form factor $A(Q_1^2,Q_2^2)$ obtained in hard wall and Sakai-Sugimoto models were used to calculate contribution to anomalous magnetic moment of muon. Here we shall take a more phenomenological approach and try to parametrize the form factors in terms of simple functional forms motivated by physical arguments such as vector dominance model or asymptotic pQCD behavior of transition form factors (see, e.g., [30]).

The behavior of transition form factors at asymptotic may be another important issue [31]. Where the pQCD sets in is interesting but still an open issue. It was discussed in [2] that for $\gamma^*\gamma^*\eta_c$ coupling this happens at very high virtualities. We leave this issue for the $\gamma^*\gamma^*f_1$ coupling for a future study.

D. $e^+e^-\to e^+e^-f_1$ reaction

The amplitude for the $e^+e^-\to e^+e^-f_1$ reaction (see Fig. 2) in high-energy approximation can be written as:

$$\mathcal{M}^{\alpha} = e(p_1+p_1')^{\mu_1}\left(\frac{ig_{\mu_1\nu_1}}{t_1}\right)T^{\nu_1\nu_2\alpha}_{\gamma^*\gamma^*\to f_1}e(p_2+p_2')^{\mu_2}\left(\frac{ig_{\mu_2\nu_2}}{t_2}\right). \tag{2.33}$$

Above $e^2 = 4\pi\alpha_{em}$. The four-momenta are defined in Fig. 2. The $T^{\nu_1\nu_2\alpha}$ vertex function responsible for the $\gamma^*\gamma^* \to f_1$ coupling was discussed in detail in the previous subsection.

The square of the matrix element, summed over polarizations of f_1, can be obtained as:

$$\overline{|\mathcal{M}|^2} = \sum_{\alpha_1,\alpha_2}\mathcal{M}^{\alpha_1}\mathcal{M}^{\alpha_2}P_{\alpha_1\alpha_2}(p_{f_1}), \tag{2.34}$$

where P is spin-projection operator for spin-1 massive particle:

$$P_{\alpha_1\alpha_2} = -g_{\alpha_1,\alpha_2} + \frac{p_{\alpha_1}p_{\alpha_2}}{M^2_{f_1}}. \tag{2.35}$$

The cross section for the 3-body reaction $e^+e^- \to e^+e^-f_1(1285)$ can be written as

$$d\sigma = \frac{1}{2s}\overline{|\mathcal{M}|^2}\cdot d^3PS. \tag{2.36}$$

The three-body phase space volume element reads

$$d^3PS = \frac{d^3p_1'}{2E_1'(2\pi)^3}\frac{d^3p_2'}{2E_2'(2\pi)^3}\frac{d^3P_M}{2E_M(2\pi)^3}\cdot(2\pi)^4\delta^4(p_1+p_2-p_1'-p_2'-P_M). \tag{2.37}$$

The phase-space for the $pp \to ppf_1$ reaction has four independent kinematical variables. In our calculation we integrate over $\xi_1 = \log_{10}(p_{1t})$, $\xi_2 = \log_{10}(p_{1t})$, azimuthal angle between positron and electron and rapidity of the produced axial-vector meson (four-dimensional integration). Here p_{1t} and p_{2t} are transverse momenta of outgoing positron and electron, respectively.

In the case of holographic approach first the $A(Q_1^2, Q_2^2)$ form factor entering the central vertex function [see Eq. (2.33)] is calculated on a two-dimensional grid and then the grid is used for interpolation for each phase space point [see (2.36)].

E. Helicity dependent $\gamma^*\gamma^* \to f_1$ vertices

As will be discussed in the result section the cross sections for the $e^+e^- \to e^+e^-f_1$ reaction presented in this paper strongly depend on functional form of the $\gamma^*\gamma^* \to f_1$ vertices as well as corresponding form factor. This is partly related to the helicity structure of vertices. In the following we will present also helicity decomposition of the $\gamma^*\gamma^* \to f_1$ vertices. The helicity-dependent matrix elements can be calculated from

$$V(\lambda_1,\lambda_2,\lambda) = \epsilon_\mu(q_1,\lambda_1)\epsilon_\nu(q_2,\lambda_2)\epsilon^*_\alpha(p,\lambda)T^{\mu\nu\alpha}(q_1,q_2). \tag{2.38}$$

The polarization vectors used here fulfill the following relations:

$$\begin{aligned} q_1^\mu\epsilon_\mu(q_1,\lambda_1) &= 0,\\ q_2^\nu\epsilon_\nu(q_2,\lambda_2) &= 0,\\ p^\alpha\epsilon_\alpha(p,\lambda) &= 0. \end{aligned} \tag{2.39}$$

$V(\lambda_1,\lambda_2,\lambda)$ is in general a complex number. For virtual photons both transverse and longitudinal photons are possible.

The result simplify in the f_1 rest frame for which:

$$q_1(E_1,0,0,q), \qquad q_2(E_2,0,0,-q) \tag{2.40}$$

and $q_1^2 = E_1^2 - q^2$, $q_2^2 = E_2^2 - q^2$, $(q_1+q_2)^2 = m_{f_1}^2$.

In the result section we shall show $V(\lambda_1,\lambda_2,\lambda)$ as a function of $Q_1^2 = -q_1^2$ and $Q_2^2 = -q_2^2$ for a few models discussed here.

From symmetry we expect only three independent $V_{TT}(Q_1^2,Q_2^2)$, $V_{LT}(Q_1^2,Q_2^2)$ and $V_{TL}(Q_1^2,Q_2^2)$ two-dimensional functions. One could also show:

$$\begin{aligned} R_{LT}(Q_1^2,Q_2^2) &= |V_{LT}(Q_1^2,Q_2^2)/V_{TT}(Q_1^2,Q_2^2)|,\\ R_{TL}(Q_1^2,Q_2^2) &= |V_{TL}(Q_1^2,Q_2^2)/V_{TT}(Q_1^2,Q_2^2)|. \end{aligned} \tag{2.41}$$

III. NUMERICAL PREDICTIONS

A. Low Q_1^2, Q_2^2 region

In Fig. 4 we show a two-dimensional distribution (ξ_1, ξ_2) of the full phase space cross section. Quite large cross sections are obtained for small ξ_1 and/or ξ_2. In addition, the different models of the $\gamma^*\gamma^*f_1$ couplings lead to very different results for the total cross section. The measurement of the total cross section is, however, rather difficult. We show both results for the original OPV model [6] as well as results modified by an extra form factor simulating not included pQVD effects to be explained below.

In Fig. 5 we show distributions in (t_1, t_2) (four-momenta squared of the virtual photons as shown in Fig. 2). Clearly some couplings generate strongly enhanced cross section at small $|t_1|, |t_2|$. The original OPV model gives unexpectedly

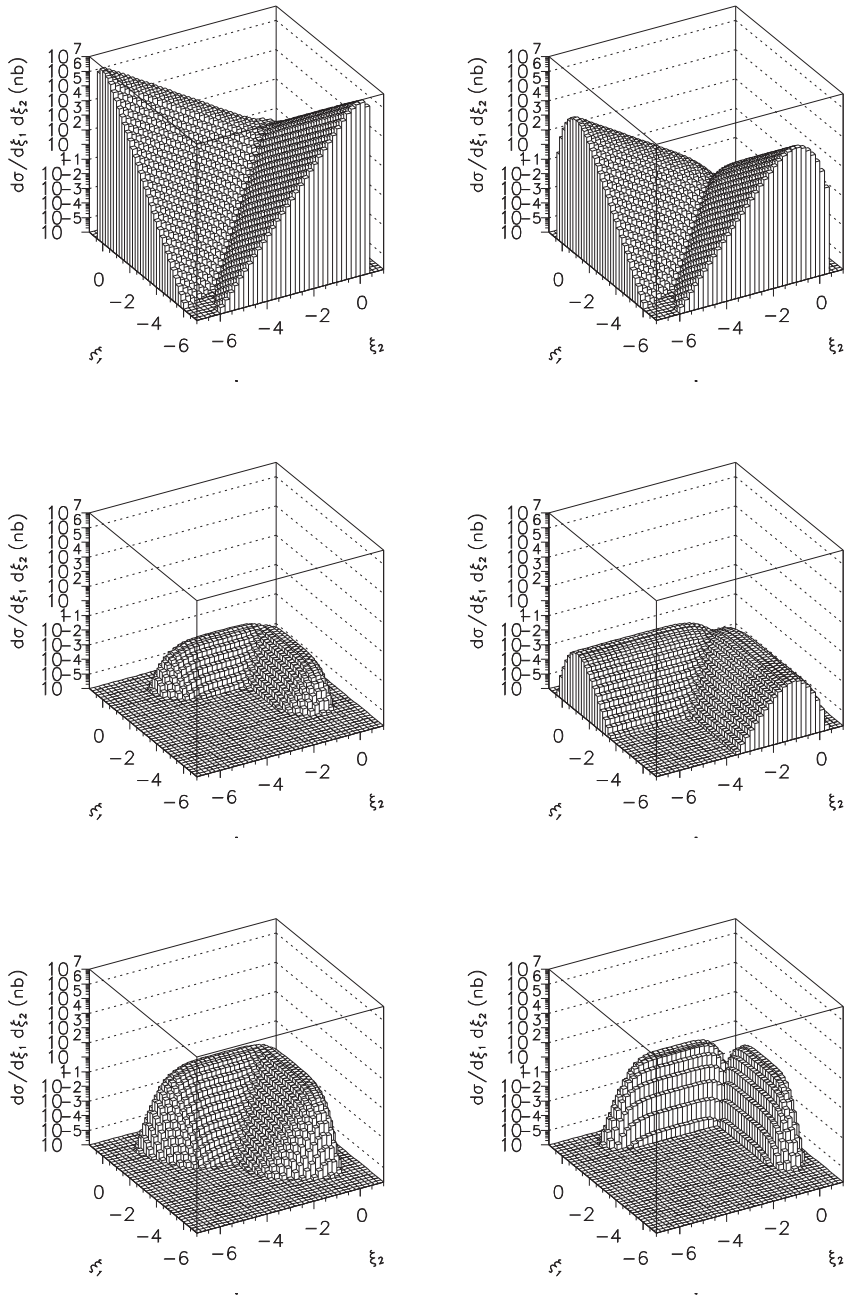

FIG. 4. Distributions in ξ_1 and ξ_2 for $\sqrt{s} = 10.5$ GeV. Here the original OPV, modified OPV, NQM, LLNRS, LR, and RS vertices were used.

large cross section at large $|t_1|$ and $|t_2|$ especially when compared to other models. The "modified OPV" means the original OPV vertex multiplied by an extra form factor:

$$F_{\text{extra}}(Q_1^2, Q_2^2) = M_{f_1}^4/(M_{f_1}^2 + Q_1^2 + Q_2^2)^2. \quad (3.1)$$

Such a form factor may simulate pQCD effects related to the quark-antiquark wave function not included in the original NJL model. Such wave function effects were included, e.g., for the pseudoscalar charmonium [3] and are crucial to describe η_c transverse momentum distribution measured recently by the LHCb collaboration. We will continue the discussion on the wave function effect in the context of double tagging.

Clearly those different vertices lead to different cross sections even for very small photon virtualities where the cross section is relatively large. Could one measure inclusive cross section for production of axial-vector meson

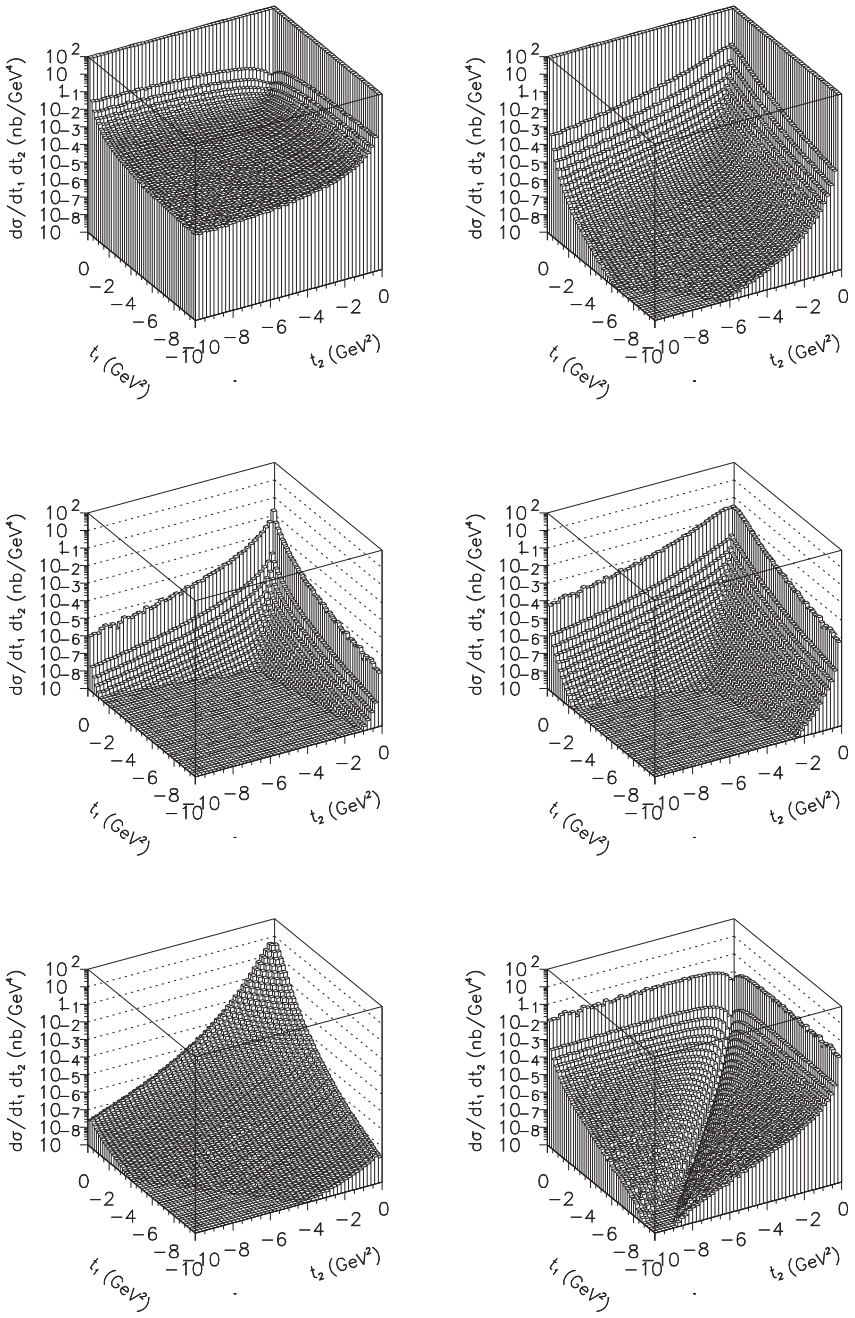

FIG. 5. Distributions in t_1 and t_2 for $\sqrt{s} = 10.5$ GeV. Here the original OPV, modified OPV, NQM, LLNRS (modified VDM), LR, and RS vertices were used.

without tagging ? Is then $\gamma^*\gamma^* \to f_1(1285)$ the dominant mechanism ? If yes, such measurements would verify the different vertices used in calculating δa_μ (axial-vector meson contribution to a_μ). Small Q_1^2 and Q_2^2 means small transverse momenta of $f_1(1285)$. Can one then identify $f_1(1285)$. Which channel is the best ? This requires further Monte Carlo studies. The resonant $e^+e^- \to f_1(1285)$ production is very small [17] and important only at resonance energies ($\sqrt{s} \sim m_{f_1}$). We are not aware about other competitive reaction mechanisms in e^+e^- collisions.

In general, one observes a strong enhancement of the $e^+e^- \to e^+e^- f_1(1285)$ cross section at $Q_1^2, Q_2^2 \to 0$ which is dictated by the singular behavior of photon propagators

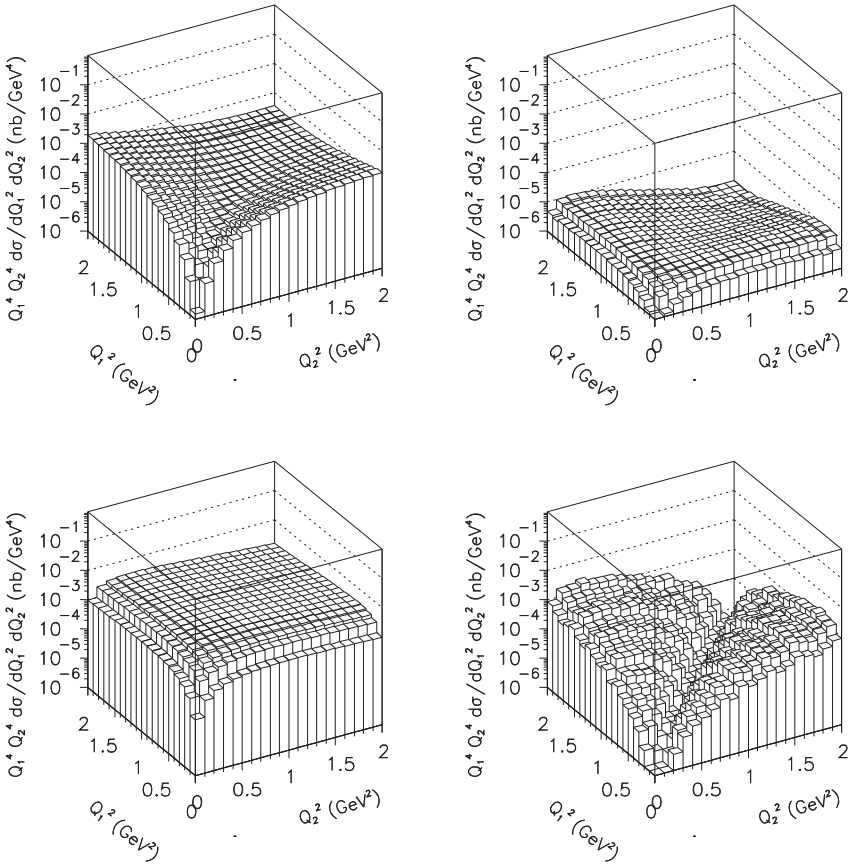

FIG. 6. A two-dimensional maps of the special quantity Ω_{LY} for $\sqrt{s} = 10.5$ GeV. Here the OPV (left upper), NQM (right upper), LR (left lower) and RS (right lower) vertices were used.

in (2.33). To illustrate and explore the effect of Landau-Yang vanishing of $T^{\mu\nu\alpha}$ vertex function for $\gamma^*\gamma^* \to f_1$ in Fig. 6 we plot the following quantity:

$$\Omega_{LY}(Q_1^2, Q_2^2) = \frac{Q_1^4 Q_2^4}{M_0^4 M_0^4} \frac{d\sigma(Q_1^2, Q_2^2)}{dQ_1^2 dQ_2^2}. \tag{3.2}$$

The arbitrary scale M_0 is chosen to be $M_0 = 1$ GeV in the following.

One can clearly see vanishing of the special quantity (3.2) at $Q_1^2 \to 0$ and $Q_2^2 \to 0$ which reflects Landau-Yang theorem. Slightly different approach patterns to zero can be observed for the different couplings. For the RS coupling we observe deep valley around $Q_1^2 = Q_2^2$ which is a direct consequence of the specific form factor used there. In this case Ω_{LY} is much smaller than for other vertices in the limited range of Q_1^2 and Q_2^2 shown in the figure.

B. Double-tagging case

In Table I we show integrated cross sections in nb for different couplings discussed in the previous section. Here we imposed only Lorentz invariant cuts $Q_1^2, Q_2^2 > 2$ GeV^2.

TABLE I. Integrated cross section in nb for the double-tagging case with $Q_1^2, Q_2^2 > 2$ GeV^2. The MR+, MR− below show the effect of interference due to sign changing of a "subleading" contribution.

Vertex	Cross section	Comment
LR	0.6892(−04)	Fact. dipole, $\Lambda = 1$ GeV
	0.3715(−04)	HW2 form factor
OPV	0.1514(+01)	Formula (30) in [6]
OPV	0.9212(−04)	Extra pQCD dipole, $\Lambda = M_{f_1}$
NQM	0.4905(−07)	Factorized dipole $\Lambda = 1$ GeV
RS	0.2138(−02)	Antisymmetric form factor, $\Lambda = 0.8$ GeV
MR +	0.4327(−07)	Symmetric and antisymmetric form factors
MR −	0.7410(−07)	Symmetric and antisymmetric orm factors
MR first	0.3432(−07)	Antisymmetric form factors
MR second	0.2435(−07)	Symmetric form factor
LLNRS	0.2666(−06)	$\Lambda_D = 1.2$ GeV, $g_{VVf_1} = 10.0$, naive VDM
LLNRS	0.1681(−05)	$\Lambda_D = 1.2$ GeV, $g_{VVf_1} = 10.0$, modified VDM

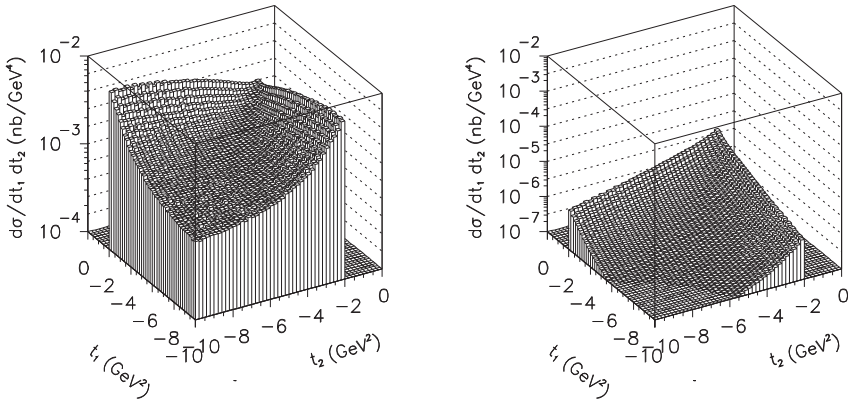

FIG. 7. The distribution in (t_1, t_2) for the OPV approach. The left panel shows result from formula (30) in [6] while the right panels shows result modified by an extra form factor simulating the f_1 wave function effects.

Quite different values are obtained with different couplings which show huge uncertainties of our predictions. Surprisingly small cross sections are obtained with the MR2019 couplings, where we show results with different sign of the second term. Therefore we show also contributions of individual terms for some couplings from the literature. They give contributions of quite different magnitude.

The results are strongly dependent on both the functional form of the vertex and on the form factor used in the calculation which is discussed below. For the OPV approach the form factor comes from the evaluation of the triangle diagram. In that approach meson couples to quarks/antiquarks in a pointlike fashion. Such an approach was questioned in [3] where it was shown that inclusion of the meson wave function is crucial to describe the $pp \to \eta_c$ data via gluon-gluon fusion. With the pointlike coupling we get gigantic cross section for the proposed DT e^+e^- experiment. Therefore we decided to "correct" this result by an extra form factor which simulates the wave function effects. Of course such a procedure is quite arbitrary but including only the triangle loop at high photon virtualities seems highly unsatisfactory, also for differential distributions. In Fig. 7 we show the result without (left panel) and with (right panel) the extra form factor.

TABLE II. Integrated cross section in nb for $e^+e^- \to e^+e^- f_1(1285)$ at $\sqrt{s} = 10.5$ GeV for the vertex used in [9] for arbitrarily changed form factors. We present results for different values of form factor parameter.

pQCD dipole Λ (GeV)	σ (nb)	Factorized dipole Λ (GeV)	σ (nb)
0.8	0.4477(−3)	0.8	0.4292(−5)
1.0	0.2236(−2)	1.0	0.6892(−4)
1.2	0.7867(−2)	1.2	0.5432(−3)

In Table II we show integrated cross section for a simple LR2019 coupling [9] supplemented by the pQCD or factorized dipole form factor with different values of the form factor parameter Λ. The results dramatically depend on the value of Λ. In addition for the same Λ the pQCD and factorized dipole Ansätze give cross section for double tagged case differing by an order of magnitude. In contrast for single tagged case they give almost the same result.

Now we wish to show several differential distributions for the double-tagged mode. In Fig. 8 we show distributions in rapidity and transverse momentum of $f_1(1285)$, t_1 or t_2, azimuthal angle between outgoing electrons, averaged virtuality

$$Q_a^2 = (Q_1^2 + Q_2^2)/2 \tag{3.3}$$

and the asymmetry parameter

$$\omega = \frac{Q_1^2 - Q_2^2}{Q_1^2 + Q_2^2}. \tag{3.4}$$

The Bose symmetry requires that:

$$\frac{d\sigma}{d\omega}(\omega) = \frac{d\sigma}{d\omega}(-\omega). \tag{3.5}$$

Quite different distributions are obtained for the different vertices used recently in the literature. Especially interesting are distribution in relative azimuthal angle between outgoing electrons and distribution in virtuality asymmetry ω. For the RS2019 vertex [8] the vanishing of the cross section for $\omega = 0$ is a consequence of the asymmetric form factor which goes to 0 for $Q_1^2 = Q_2^2$. With the RS2019 vertex axial vector mesons do not contribute to the hyperfine splitting of muonic atoms. It is obvious that the DT measurements of distributions shown in Fig. 8 would

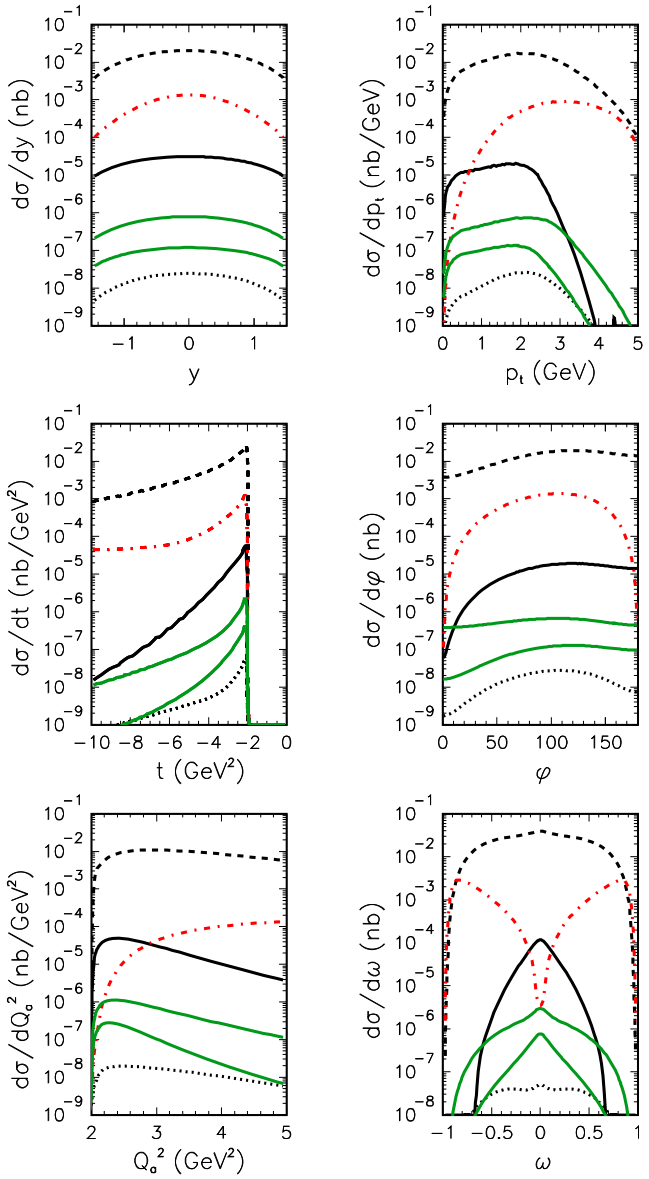

FIG. 8. Several distributions for production of $f_1(1285)$ in double-tagging mode with $Q_1^2, Q_2^2 > 2$ GeV^2. The solid line is for LR, the dashed line for modified OPV, the dotted line for NQM, the dash-dotted line for RS vertex and the green dash-dotted lines are for LLNRS vertices (lower—naive VDM, upper—modified VDM).

provide strong limitations on the vertices used in calculating fundamental quantities such as muon anomalous magnetic moment a_μ and/or hyperfine splitting of muonic hydrogen.

C. Helicity dependent matrix elements

We have shown that the different models presented in the literature give very different results, especially for larger photon virtualities Q_1^2 and/or Q_2^2. To illustrate the situation better here we shall show also helicity-dependent matrix elements for a few models.

In principle, there are many $(\lambda_1\lambda_2\lambda)$ amplitudes that depend on both photon virtualities. The symmetries and the structure of the vertices infer that only a few are really independent. For example we find:

$$\begin{aligned} |V(+1,0,+1)| &= |V(0,-1,+1)| \\ &= |V(-1,0,-1)| \\ &= |V(0,+1,-1)|. \end{aligned} \tag{3.6}$$

The different matrix elements can be classified into TT, LT, TL components, where T and L denote transverse and longitudinal photons.

In Fig. 9 we show V_{LT}, V_{TL}, and V_{TT} as a function of photon virtualities Q_1^2 and Q_2^2 for a few examples of models: OPV (upper row), NQM (middle row), and LNSS (lower row). We observe very different dependence of the matrix elements (supplemented by form factors) on Q_1^2 and Q_2^2. Also the relative size of the LT, TL, and TT terms depends on the model. While in the OPV model the TL + LT contributions are much larger than the TT contribution for the NQM model all components are of similar size.

In the LLNRS model there is not at all TT contribution. We see that in this model only TL and LT terms occur. So at least one photon is longitudinal. In this case the simple formula (2.22) may not be appropriate. As discussed, e.g., in [32] the form factors for both terms in (2.22) should be rather of the type:

$$\frac{m_V^2}{m_V^2+Q_1^2}\cdot\xi_V\sqrt{\frac{Q_2^2}{m_V^2}}\frac{m_V^2}{m_V^2+Q_2^2},$$
$$\xi_V\sqrt{\frac{Q_1^2}{m_V^2}}\frac{m_V^2}{m_V^2+Q_1^2}\cdot\frac{m_V^2}{m_V^2+Q_2^2} \tag{3.7}$$

for the first (TL) and second (LT) term, respectively, different for each term. The constant ξ_V is known phenomenologically to be of the order of 1. Therefore in our calculation we shall use also result of the slightly modified model inspired by the $VV \to f_1$ LLNRS vertex. The results were already presented in Table 1 and Fig. 8. The cross sections for the modified vertex are larger than the naive one [see (2.22)] for the DT kinematics. The reader is asked to note zeroing of V_{TT} for $Q_1^2 = Q_2^2$ for the presented models. This is a general future related to the boson symmetry.

In Fig. 10 we show LT and TL contributions for the LNSS model for the two different VDM prescriptions. The result for the modified prescription is very different from that for the naive prescription.

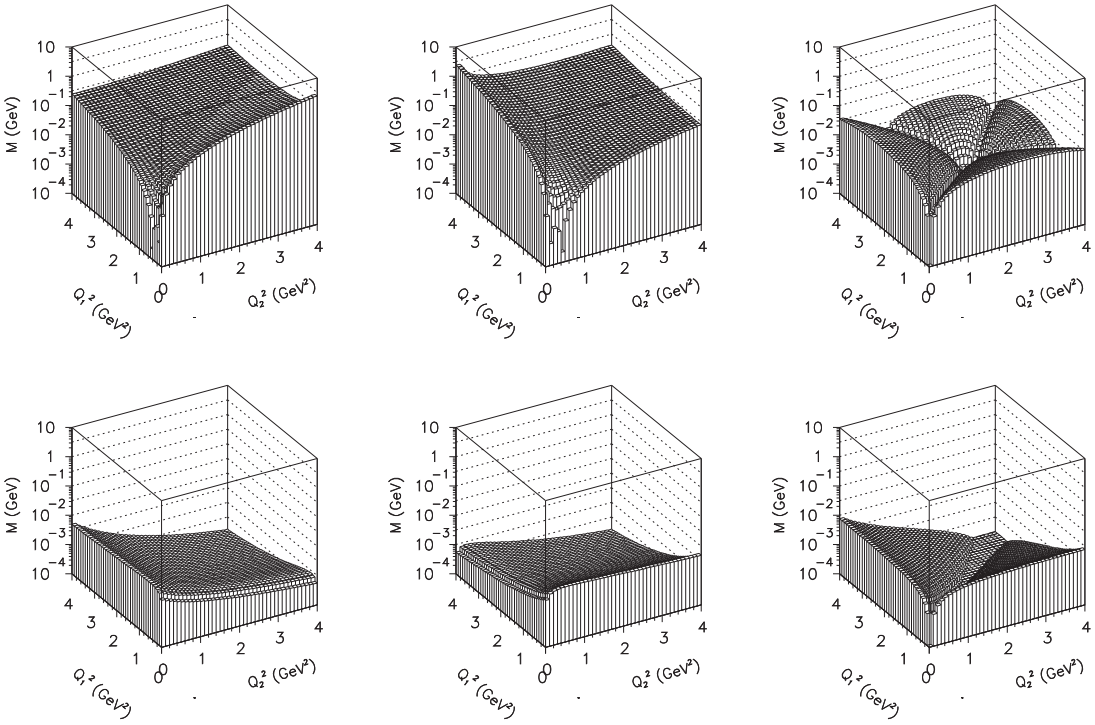

FIG. 9. $|V_{LT}|$, $|V_{TL}|$, and $|V_{TT}|$ for OPV (upper low) and NQM (lower row) models of the $\gamma\gamma \to f_1$ coupling.

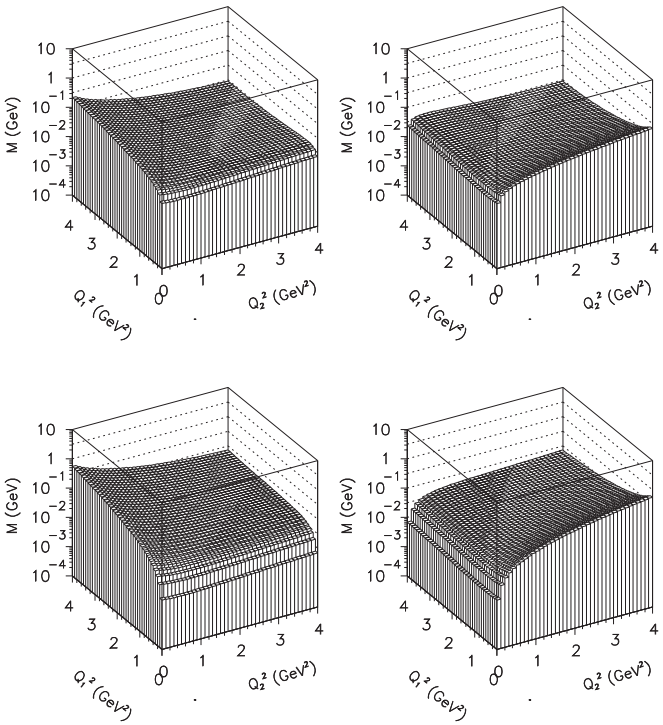

FIG. 10. $|V_{LT}|$ and $|V_{TL}|$ for the naive LLNRS (upper low) and modified LNNRS (lower row) models of the $\gamma\gamma \to f_1$ coupling.

IV. CONCLUSIONS

In this paper the results of calculations of cross sections and differential distributions for the $e^+e^- \to e^+e^- f_1(1285)$ have been performed using different $\gamma^*\gamma^* \to f_1(1285)$ couplings known from the literature. These couplings were used previously to calculate hadronic light-by-light axial-vector meson contributions to anomalous magnetic moment of muon as well as for hyperfine splitting of the muon hydrogen.

We have presented predictions relevant for future double-tagged experiments for Belle II. The results strongly depend on the details of calculation (type of tensorial coupling and/or form factors used). The form factor cannot be reliably calculated at present. We have presented several differential distributions in photon virtualities, transverse momentum of $f_1(1285)$, distribution in azimuthal angle between outgoing electron and positron and so-called asymmetry of virtualities (ω). Especially the latter observable (asymmetry) seems promising for verifying the quite different models of the $\gamma^*\gamma^*AV$ coupling. The results strongly depend on details of the coupling(s). The double tagged measurement would therefore be very valuable to constrain the couplings and form factors and in a consequence would help to decrease uncertainties of their contribution to anomalous magnetic moment of muon and hyperfine splitting of muonic hydrogen.

To illustrate the differences between various models used in the literature in the context of muon anomalous moment

we have presented also the helicity dependent matrix elements for the $\gamma^*\gamma^* \to f_1$ vertex as a function of photon virtualities. The matrix elements for different models show very different behaviour on the two-dimensional (Q_1^2, Q_2^2) plane. This is another interesting representation of the models, however rather difficult for experimental verification.

In the present models the form factors attached to vertices are a bit arbitrary and can be reasonable only for small values of Q_1^2 and Q_2^2. The Belle II experiment could provide direct information how they look like as a function of both photon virtualities. The nonlocal coupling via triangle loop is, in our opinion, also not sufficient at larger values of Q_1^2, Q_2^2 relevant for the DT experiment. The present situation calls for calculation of such form factors using "realistic" momentum space quark-antiquark wave function. This may be not an easy task and requires a development of the relevant formalism.

Both $\eta\pi^+\pi^-$ (as in [23]) as well as $\pi^+\pi^-\pi^+\pi^-$ (used recently at the LHC [33]) channels could be applied experimentally to identify the $f_1(1285)$ meson. The $\eta\pi^+\pi^-$ option is dangerous as there is another meson close by which decays to the same decay channel: $\eta(1295) \to \eta\pi\pi$ [34]. This meson may be also abundantly produced in $\gamma\gamma$ fusion as $\Gamma_{\eta'\to\gamma\gamma} = 4.27$ keV [35]. $f_1(1285) \to \rho^0\gamma$ with BR $= 5.3\%$ [29] would be another possible choice. The decays of light axial vector mesons were discussed, e.g., in [36–38].

In the present paper we concentrated on production of $f_1(1285)$ meson. A similar analysis could be performed for other axial-vector mesons such as $a_1(1260)$ or $f_1(1420)$. Then coupling constants and some form factors must be changed in the calculation. On the experimental side, decay channels specific for a given meson must be selected.

The production of isoscalar axial-vector mesons is very interesting also in the context of central exclusive processes $pp \to ppf_1$. There the unknown ingredient is Pomeron-Pomeron-f_1 vertex. This is discussed elsewhere [25].

ACKNOWLEDGMENTS

I am indebted to Wolfgang Schäfer for collaboration on quarkonium production in photon-photon collisions and Piotr Lebiedowicz for collaboration on diffractive production of f_1 meson. The discussion with Anton Rebhan, Josef Leutgeb, Alexander Osipov, Pablo Roig, and Pablo Sanchez-Puertas and Sasha Dorokhov on $\gamma^*\gamma^* \to f_1(1285)$ vertices and with Alexander Rudenko about $f_1(1285) \to e^+e^-$ is acknowledged. The symmetry relations were discussed with Otto Nachtmann. The decays of f_1 and related difficulties were discussed with Nikolay Achasov. A possibility of a measurement at Belle II was discussed with Sadaharu Uehara. This study was partially supported by the Polish National Science Center Grant No. UMO-2018/31/B/ST2/03537 and by the Center for Innovation and Transfer of Natural Sciences and Engineering Knowledge in Rzeszów.

[1] G. Köpp, T. V. Walsh, and P. Zerwas, Nucl. Phys. **B70**, 461 (1974).
[2] I. Babiarz, V. Goncalves, R. Pasechnik, W. Schäfer, and A. Szczurek, Phys. Rev. D **100**, 054018 (2019).
[3] I. Babiarz, R. Pasechnik, W. Schäfer, and A. Szczurek, J. High Energy Phys. 06 (**2020**) 101; arXiv:2002.09352.
[4] V. Pascalutsa, V. Pauk, and M. Vanderhaeghen, Phys. Rev. D **85**, 116001 (2012).
[5] V. Pauk and M. Vanderhaeghen, Eur. Phys. J. C **74**, 3008 (2014).
[6] A. A. Osipov, A. A. Pivovarov, and M. K. Volkov, Phys. Rev. D **96**, 054012 (2017).
[7] A. E. Dorokhov, A. P. Martynenko, F. A. Martynenko, A. E. Radzhabov, and A. S. Zhevlakov, EPJ Web Conf. **212**, 05001 (2019).
[8] P. Roig and P. Sanchez-Puertas, Phys. Rev. D **101**, 074019 (2020).
[9] J. Leutgeb and A. Rebhan, Phys. Rev. D **101**, 014006 (2020).
[10] L. Cappiello, O. Cata, G. D'Amrosio, D. Greynat, and A. Iyer, Phys. Rev. D **102**, 016009 (2020).
[11] F. Jegerlehner and A. Nyffeler, Phys. Rep. **477**, 1 (2009).
[12] F. Jegerlehner, Springer Tracts Mod. Phys. **274**, 1 (2017).
[13] J. S. Schwinger, Phys. Rev. **73**, 416 (1948).
[14] T. Aoyama *et al.*, Phys. Rep. **887**, 1 (2020).
[15] A. E. Dorokhov, N. I. Kochelev, A. P. Martynenko, F. A. Martynenko, and A. E. Radzhabov, Phys. Lett. B **776**, 105 (2018).
[16] A. S. Rudenko, Phys. Rev. D **96**, 076004 (2017).
[17] A. I. Milstein and A. S. Rudenko, arXiv:1909.07938; Phys. Lett. B **800**, 135117 (2020).
[18] M. N. Achasov *et al.* (SND collaboration), Phys. Lett. **800**, 135074 (2020).
[19] R. Dickson *et al.* (CLAS collaboration), Phys. Rev. C **93**, 065202 (2016).
[20] N. I. Kochelev, M. Battaglieri, and R. DeVita, Phys. Rev. C **80**, 025201 (2009).
[21] S. K. Domokos, H. R. Grigoryan, and J. A. Harvey, Phys. Rev. D **80**, 115018 (2009).
[22] Y. Huang, J.-J. Xie, X.-R. Chen, J. He, and H.-F. Zhang, Int. J. Mod. Phys. E **23**, 140002 (2014).
[23] P. Achard *et al.* (L3 collaboration), Phys. Lett. B **526**, 269 (2002).
[24] P. Masjuan, P. Roig, and P. Sanchez-Puertas, arXiv: 2005.11761.

[25] P. Lebiedowicz, J. Leutgeb, O. Nachtmann, A. Rheban, and A. Szczurek, arXiv:2008.07452.
[26] P. Lebiedowicz, O. Nachtmann, P. Salabura, and A. Szczurek (to be published).
[27] C. Ewerz, M. Maniatis, and O. Nachtmann, Ann. Phys. (Amsterdam) **342**, 31 (2014).
[28] L. D. Landau, Dokl. Akad. Nauk Ser. Fiz **60**, 207 (1948); C. N. Yang, Phys. Rev. **77**, 242 (1950).
[29] M. Tanabashi *et al.* (Particle Data Group), Phys. Rev. D **98**, 030001 (2018).
[30] M. Diehl, P. Kroll, and C. Vogt, Eur. Phys. J. C **22**, 439 (2001).
[31] M. Hoferichter and P. Stoffer, J. High Energy Phys. 05 (2020) 159.
[32] D. Schildknecht, G. A. Schuler, and B. Surrow, Phys. Lett. B **449**, 328 (1999).
[33] E. Bols, Master thesis, Copenhagen University, 2017. The thesis is available at http://cds.cern.ch/record/2288372/files/CERN-THESIS-2017-175.pdf.
[34] N. Achasov (private communication).
[35] A. V. Anisovich, V. V. Anisovich, L. Montanet, and V. A. Nikonov, Eur. Phys. J. A **6**, 247 (1999).
[36] L. Roca, J. E. Palomar, and E. Oset, Phys. Rev. D **70**, 094006 (2004).
[37] L. Roca, A. Hosaka, and E. Oset, Phys. Lett. B **658**, 17 (2007).
[38] K. Chen, Ch.-Q. Pang, X. Liu, and T. Matsuki, Phys. Rev. D **91**, 074025 (2015).